



## AN X-RAY DIFFRACTION STUDY OF PMN-PT CERAMICS NEAR THE MORPHOTROPIC PHASE BOUNDARY

H.W. KING,<sup>1</sup> S.H. Ferguson,<sup>1</sup> D.F. Waechter,<sup>2</sup> and S.E. Prasad<sup>2</sup>

<sup>1</sup>Department of Mechanical Engineering, University of Victoria, BC, V8W 3P6, Canada.

<sup>2</sup>Sensor Technology Limited, PO Box 97, Collingwood, ON, L9Y 3Z4, Canada.

**Abstract:** The temperature dependence of crystal structures and lattice parameters has been determined for compositions of  $x = 0.20, 0.30$  and  $0.35$  in the system  $(1-x)\text{PMN}-x\text{PT}$ , which has shown great potential for sonar sensor applications. The temperatures of the onset of the cubic-pseudocubic transformation in  $x = 0.20$ , and of the cubic-tetragonal transformations in  $x = 0.30$  and  $0.35$ , have been established from studies of diffraction profiles and confirmed from lattice parameter-temperature plots. As these phase changes transform progressively over ranges of temperature, the phase boundaries normally inserted in diagrams for the system should be shown as two phase regions, rather than narrow lines. On the basis of these results, the dielectric state diagrams of the PMN-PT system have been modified to produce a partial realization diagram that includes the start temperatures of the various phase transformations.

### 1. INTRODUCTION

The electrostrictive properties of ceramics with compositions in the relaxor region ( $x \leq 0.1$ ) in the solid solution  $(1-x)\text{Pb}(\text{Mg}_{1/3}\text{Nb}_{2/3})\text{O}_3-x\text{PbTiO}_3$  (PMN-PT) have been extensively investigated for actuator applications involving large voltage-induced displacements [1-4]. Ceramics with higher PT compositions ( $x = 0.30-0.35$ ) in the region of the morphotropic phase boundary (MPB) display piezoelectric properties appropriate for use in sensor applications [5-8]. Intermediate compositions ( $x = 0.1-0.24$ ), which transform from relaxor to ferroelectric behaviour at low temperatures, are also being investigated for use as transducers and sensors [9-11]. The initial application of PMN based ceramics for critical systems was troubled by inconsistent electromechanical performance, due to compositional variability and the presence of the detrimental pyrochlore phase, but these problems have now been effectively overcome by improved processing methods [12-17]. The US National Center for Excellence in Metalworking Technology (NCEMT), for example, has recently reported on the success of a program to improve the mechanical reliability of high power density PMN-based ceramics and has demonstrated the effectiveness of these materials in a Lightweight Broadband Variable Depth Sonar System [18].

A recent study of PMN-PT relaxor ferroelectrics [19] with compositions of  $x = 0.00, 0.08$  and  $0.20$  has shown that the thermal expansion coefficients increase by an order of magnitude at a well defined temperature  $T_\alpha$ , which is considerably greater than the temperature  $T_m$  at which the dielectric peak is at a maximum. As concurrent studies of diffraction profiles confirm that the onset of the pseudocubic phase transformation correlates with the temperature  $T_\alpha$ , rather than  $T_m$ , the validity of PMN-PT phase diagrams based on dielectric measurements [5,8] is open to question. To clarify the situation with respect to PMN-PT ceramics with properties appropriate for transducers and sensors, the temperature

dependence of the thermal expansion coefficients of compositions in the region of the morphotropic phase boundary has been investigated by high temperature X-ray diffraction.

## 2. EXPERIMENTAL METHODS

Specimens of (1-x)PMN–xPT, with compositions of  $x = 0.30$  and  $0.35$  were fabricated at Sensor Technology Ltd., using a direct synthesis technique [17]. An additional composition with  $x = 0.20$  was also included in the study, to provide a comparison with the previous findings on compositions that exhibit relaxor properties [19]. Proportionate amounts of the oxides of lead, magnesium and niobium to give the required compositions were ball milled to fine powder and calcined to form the mixed oxide perovskite phase. The calcined product was crushed, milled to fine powder and then pressed into disks about 25 mm diameter and 1.2 mm thick. After bisquing to remove volatile organic binders and lubricants, the disks were fired to obtain sintered ceramics, which were ground flat and cut into X-ray specimens 12.5 mm wide x 19 mm long x 1 mm thick.

X-ray diffraction experiments were performed on a Scintag XDS 2000 theta-theta X-ray diffractometer equipped with a high resolution Peltier-cooled drifted Si detector and operated at 44 kV and 40 mA using copper radiation ( $\lambda_{\text{CuK}\alpha 1} = 1.54060 \text{ \AA}$ ). A Buehler HDK 2.3 high temperature attachment was used for controlling sample temperatures between room temperature and 300°C. The samples were mounted on a specially designed stainless steel sample holder which was rigidly clamped at one end only, to permit free expansion in the plane of the specimen. To eliminate thermal gradients along the length of the specimen, the sample was heated in air using only the surround heater of the Buehler furnace and its temperature was measured and controlled to  $\pm 1 \text{ }^\circ\text{C}$ , using a Pt/Pt-13%Rh thermocouple.

For the investigation of crystal structure changes by Bragg peak splitting, selected diffraction profiles were step scanned with a step size of  $0.06^\circ$  and a relatively long dwell time of 20 seconds, to reduce the experimental scatter of the results. For lattice parameter determinations, six to nine relatively intense Bragg peaks over the angular range from  $60$  to  $141 \text{ }^\circ 2\theta$  were step scanned using a receiving slit of  $0.3^\circ$ , a step size of  $0.06^\circ$  and a dwell time of 2.5 seconds. To eliminate angular dependent instrumental and measurement errors, lattice parameters calculated from the Bragg peak positions were plotted against the function  $\cos\theta \cdot \cot\theta$  and extrapolated to  $\theta = 90^\circ$ . An equation for the linear line trend was derived for each of these plots, to obtain a lattice parameter with an estimated accuracy of  $\pm 0.0001 \text{ \AA}$  [20].

## 3. RESULTS

### Temperature Dependence of Diffraction Profiles

The room temperature X-ray diffraction patterns of the three PMN–PT samples over Bragg angles up to  $90 \text{ }^\circ 2\theta$  are shown in Fig. 1. No tetragonal splitting, or resolution of the  $\text{K}_{\alpha 1}$ - $\text{K}_{\alpha 2}$  doublets, was observed in these relatively broad low angle profiles, as shown in Fig. 1, but all of the peaks could be labeled in terms of a pseudocubic perovskite crystal structure. The absence of a significant diffraction peak in the region of  $29 \text{ }^\circ 2\theta$  also confirmed that the single stage calcination process used to fabricate the samples effectively eliminates the pyrochlore phase.

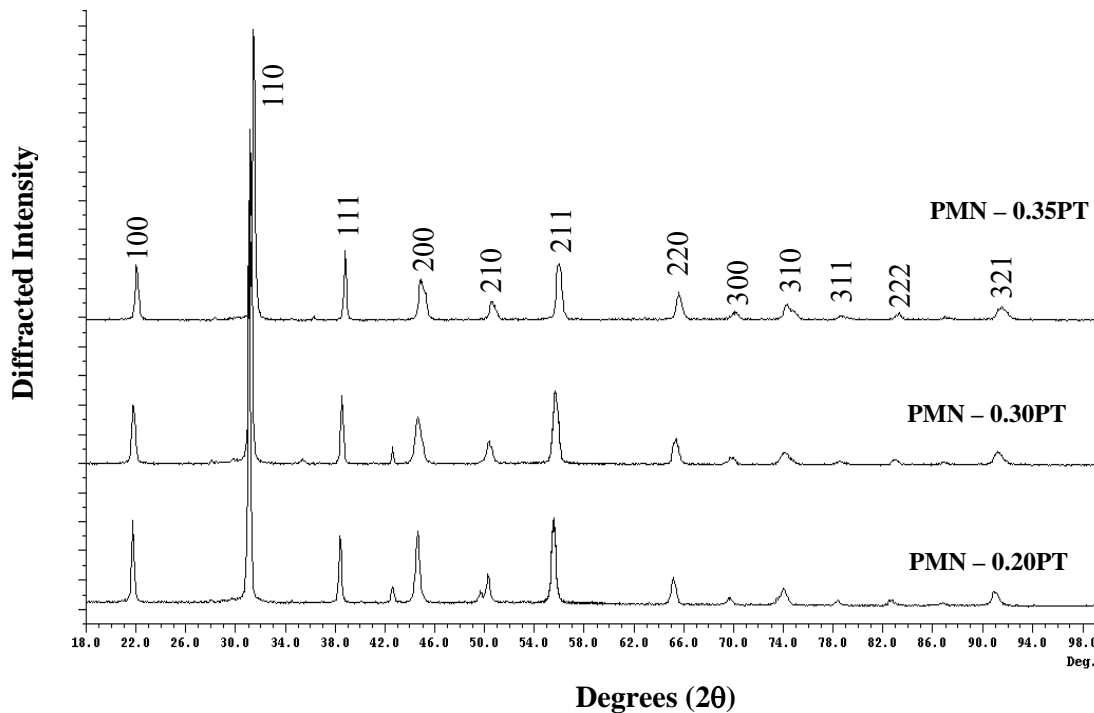


Figure 1. Room temperature diffraction patterns for specimens.

Since PMN-PT ceramics with compositions in the region of the MPB are known to undergo successive phase transformations on cooling [5,7,8], the temperature dependence of the shapes of diffraction profiles was investigated by step scanning selected Bragg peaks at intervals of approximately  $20^\circ\text{C}$  over the temperature range from room temperature to  $240^\circ\text{C}$ . As shown by the successive scans of the 332 profile of the  $x = 0.2$  relaxor sample in Fig. 2, at temperatures above  $140^\circ\text{C}$  the structure is cubic with a clear resolution of the  $K_{\alpha 1}$ - $K_{\alpha 2}$  doublet. The onset of the pseudocubic structure in this relaxor sample occurs between  $140$  and  $120^\circ\text{C}$ , as indicated by a broadening of the  $K_{\alpha 1}$  peak and the concurrent loss in resolution of the  $K_{\alpha 2}$  peak. The broadened pseudocubic profile is observed at temperatures down to  $80^\circ\text{C}$ . At temperatures between  $60^\circ\text{C}$  and room temperature, however, two further diffraction peaks become progressively resolved. The angular separation and relative intensity of these peaks is consistent with their identification as the  $3\bar{3}2$ - $3\bar{3}\bar{2}$  peaks of the low temperature rhombohedral structure [19].

The 332 cubic diffraction peak of the sample with  $x = 0.3$ , which is included in Fig. 2, exhibits a well resolved cubic  $K_{\alpha 1}$ - $K_{\alpha 2}$  profile at temperatures down to  $160^\circ\text{C}$ . Small satellite peaks observed on the shoulders of the cubic  $K_{\alpha 1}$  peak at  $140^\circ\text{C}$  are attributed to tetragonal splitting, while additional more widely separated satellite peaks observed on the lower slopes of the cubic  $K_{\alpha 1}$  peak at  $120^\circ\text{C}$  are associated with the rhombohedral structure, which forms as the sample crosses the morphotropic phase boundary between  $120$  and  $130^\circ\text{C}$ . The cubic peak becomes progressively less intense below  $100^\circ\text{C}$ , so that the dominant feature of the profile is a broad plateau with multiple small peaks. The tetragonal peaks are less pronounced at room temperature, so that the rhombohedral peaks become the dominant

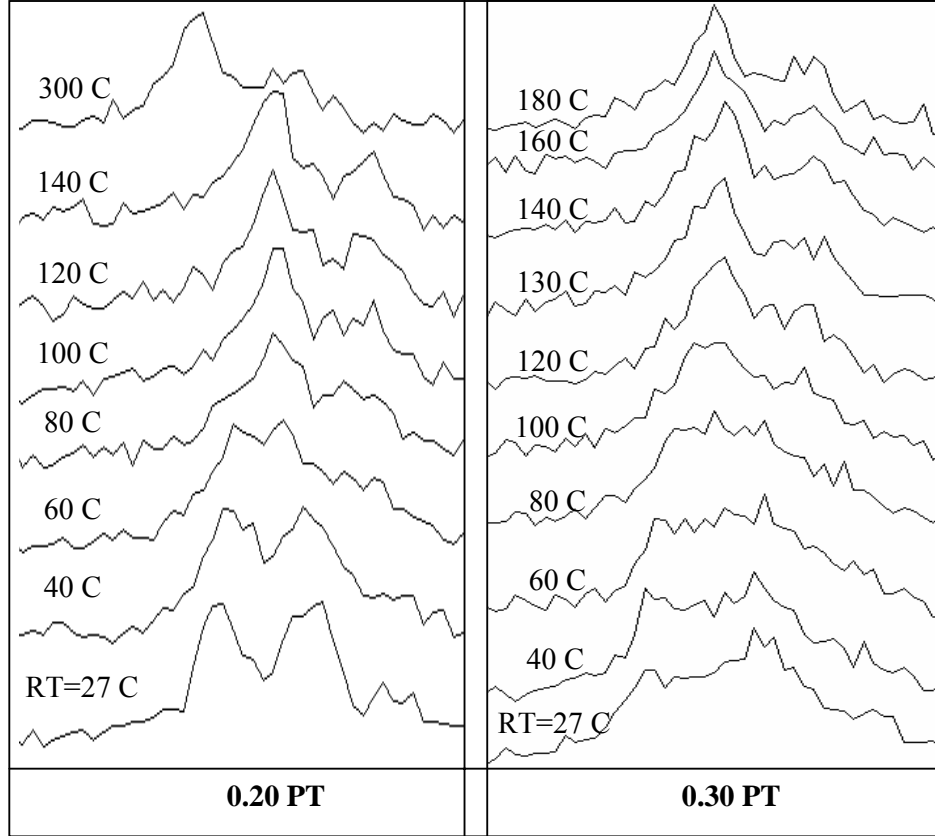


Figure 2. Temperature dependence of 332 profiles for PMN-0.20PT and PMN-0.30PT.

structural feature of the profile. Even so, the rhombohedral peaks are not as well resolved as those observed in the  $x = 0.2$  sample, in which no tetragonal structure is formed.

Fig. 3 shows that the 332 diffraction profile of the  $x = 0.35$  sample also exhibits a well resolved cubic  $K_{\alpha 1}$ - $K_{\alpha 2}$  profile at temperatures down to 200 °C, but tetragonal splitting is clearly evident at 180 °C and below. As additional satellite peaks are observed at lower temperatures, while the intensity of the cubic peak is decreased, a profile composed of multiple peaks superimposed on a broad plateau is observed at temperatures below 100 °C. In order to identify the temperature of the onset of the additional low temperature peaks, the 222 peak of this sample was step scanned over the temperature range from 160 °C down to room temperature, to obtain the results which are included in Fig. 3. Since the 222 Bragg peak does not split into a tetragonal doublet, these diffraction profiles show only a broadened  $K_{\alpha 1}$ - $K_{\alpha 2}$  peak at temperatures down to 80 °C. At 60 °C and below, the 222 peak shows splitting due to the separation of the 222 and  $\bar{2}22$  peaks of the rhombohedral structure, confirming that these peaks contribute to the multiple peaks superimposed on the broad plateau in the low temperature profile of the 332 peak, *i.e.* this sample crosses the MPB between 60 and 80 °C. These findings are in good agreement with the recent results of Kojima and Jiang [21], who report that 0.65PMN-0.35PT undergoes a cubic to tetragonal change at 158 °C and a further tetragonal to rhombohedral change at 60 °C.

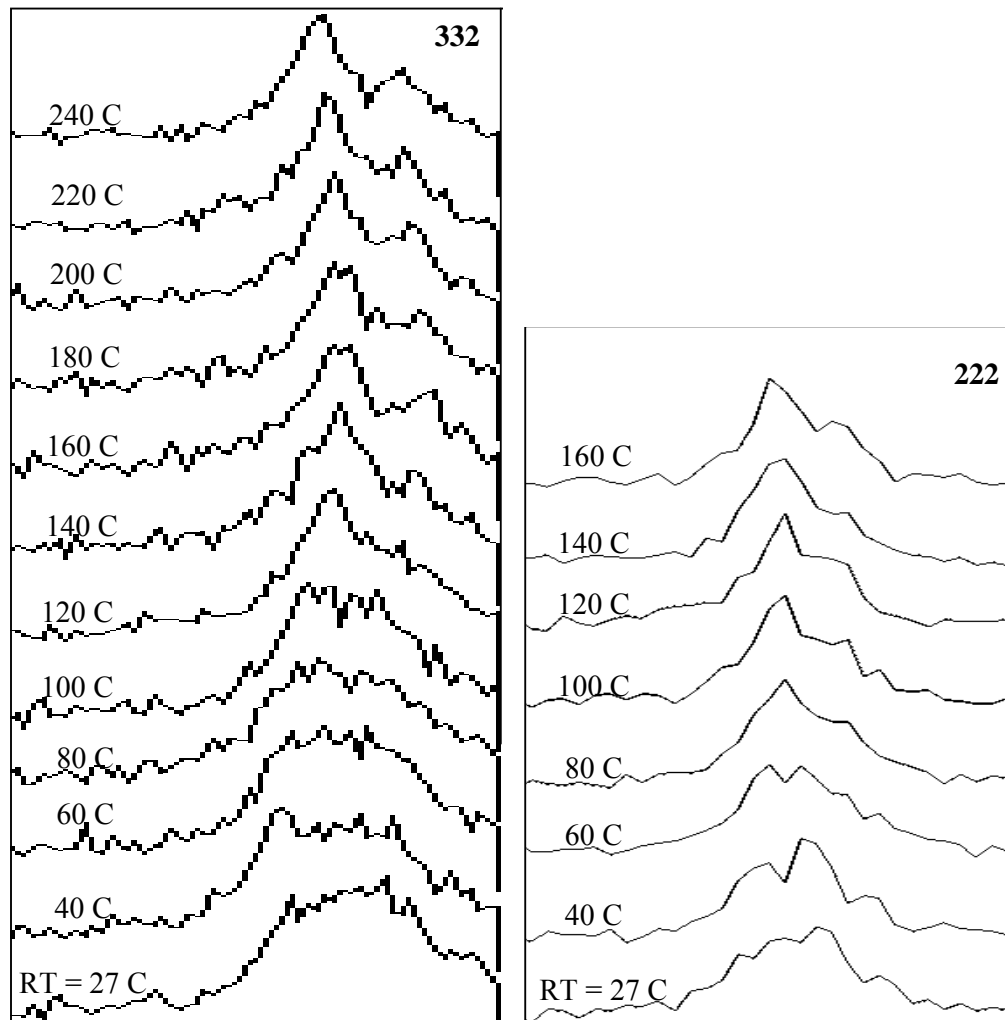


Figure 3. Temperature dependence of 332 and 222 profiles for PMN-0.35PT.

It is significant to note that broadened profiles with multiple peaks were also observed for PMN-PT samples at room temperature by Ho *et al.* [7], but these authors did not comment on these findings. However, they did report that a sample with  $x = 0.32$  had a bimodal microstructure at room temperature, composed of a small number of  $4 \mu\text{m}$  grains mixed with a larger number of  $9 \mu\text{m}$  grains, which implied the coexistence of two phases. This is perhaps the first time that it has been suggested that the phase transformations that occur in the region of the MPB do not go to completion at the temperature at which they are initiated. The progressive changes in the diffraction profiles shown in Figs. 2 and 3 also indicate that the boundaries between structural phases in the PMN-PT system, including the morphotropic phase boundary, should be regarded as two phase regions, rather than narrow lines.

#### Temperature Dependence of Lattice Parameters

Lattice parameters determined from  $K_{\alpha 1}$  Bragg peak positions measured at  $20 \text{ }^\circ\text{C}$  intervals over the range from room temperature to  $300 \text{ }^\circ\text{C}$  are plotted against temperature in Fig. 4. The high temperature plots of the cubic  $a$  lattice parameter of the samples are all strictly linear. These plots also have closely

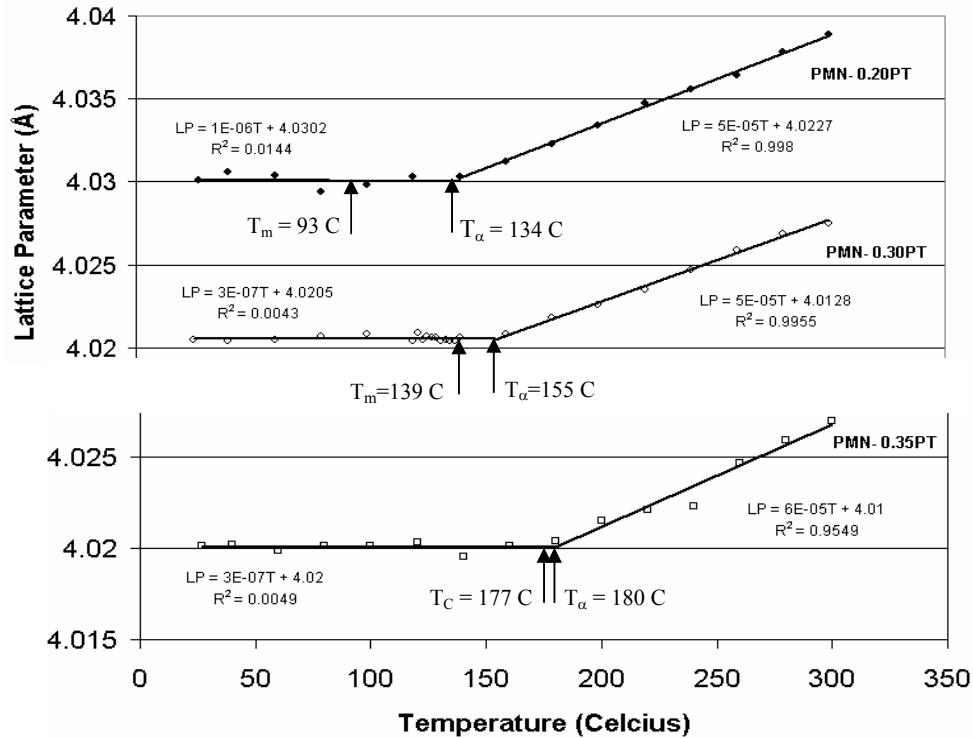


Figure 4. Lattice Parameters vs. Temperature for PMN-PT

similar slopes, indicative of relatively high thermal expansion coefficients ( $\alpha$ ) of  $5-6 \times 10^{-5}$  mm/mm per  $^{\circ}\text{C}$ . In the absence of clearly resolved crystal structures at low temperatures, the broadened  $K_{\alpha 1}$  diffraction profiles of the types shown in Fig. 2 were indexed as pseudocubic and the associated Bragg angles were derived by taking the mid-positions at half the peak height. The plots of lattice parameters determined from these broadened Bragg profiles are also strictly linear with slopes indicative of much smaller thermal expansion coefficients of  $1-3 \times 10^{-7}$  mm/mm per  $^{\circ}\text{C}$ . These results are consistent with the previous findings by Cross [22], who reported  $\alpha$  values of  $10^{-5}$  mm/mm per  $^{\circ}\text{C}$  at  $400^{\circ}\text{C}$  and  $<10^{-6}$  mm/mm per  $^{\circ}\text{C}$  at room temperature, for a sample of 0.9PMN-0.1PT. The difference between the thermal expansion coefficients of the cubic phase and the non-centrosymmetric low temperature phases can be attributed to stronger bonding in the low temperature structures, as shown by the 4% decrease in cell volume/molecule on going from the cubic to the tetragonal, orthorhombic or rhombohedral structures of  $\text{BaTiO}_3$ , while the difference in cell volumes/molecule of the low temperature structures is less than the scatter of the experimental results reported by different investigators [23].

It is also evident from Fig. 4 that the linear plots intersect at clearly defined temperatures, which are equal to 134, 155 and  $180^{\circ}\text{C}$ , for the samples with  $x = 0.2, 0.3$  and  $0.35$ , respectively. As all of these temperatures are within the respective  $20^{\circ}\text{C}$  intervals within which the diffraction profiles of the high temperature cubic phases show the onset of rhombohedral, or tetragonal, peak splitting (Figs. 2 and 3), they can be used as more precise indicators of these structural transformation temperatures. In a previous publication [19] it was reported that the  $T_{\alpha}$  temperatures obtained for PMN-PT samples of composition  $x = 0.00, 0.08$  and  $0.20$  were significantly greater than the respective temperatures of  $-18, 32$  and  $93^{\circ}\text{C}$  [5-7]. The results obtained in the present work confirm that these two parameters draw

closer together in magnitude with increasing PT content, so that for  $x = 0.30$   $T_\alpha$  is only 16 °C greater than the  $T_m$  of 139 °C [5-7], while at  $x = 0.35$   $T_\alpha$  is effectively the same as the  $T_m$  of 177 °C [5-7].

#### 4. DISCUSSION AND CONCLUSIONS

The generally accepted "phase diagrams" of the PMN-PT ceramic system [5-7] are based on the compositional dependence of dielectric measurements. While plots of parameters such as  $T_m$  may be appropriate for delineating various dielectric states, the present results, and the previous findings on relaxor samples [19], have shown that they do not necessarily represent boundaries between different structural phases. Since the  $T_\alpha$  temperatures have been shown to correlate with the onset of the cubic-pseudocubic, or cubic-tetragonal phase transformations, it is of interest to plot these points on the "phase diagram" of the PMN-PT system developed by Choi *et al.* [5] using measurements of  $T_m$ . As shown in Fig. 5, the  $T_\alpha$  plot deviates significantly from the  $T_m$  plot in the region of the cubic-pseudocubic transformation at low PT compositions, but the two plots merge together in the region of the morphotropic phase transformation and thereafter follow closely similar trends in the region of the cubic-tetragonal phase transformation. It would be of interest to determine whether this coincidence continues to the higher PT compositions that display piezoelectric characteristics. In previous diagrams, the morphotropic boundary between the low temperature non-centrosymmetric tetragonal and rhombohedral phases is shown as a vertical cut off, at a composition of  $x = 0.3$  [5], or  $x = 0.35$  [7]. However, the present admittedly limited data, which do have positive support from recent broadband Brillouin scattering measurements [21], indicate that this boundary has a distinct negative slope, so that small amounts of the tetragonal phase may transform to the rhombohedral phase even at compositions beyond  $x = 0.35$ .

The previous results on lower PT compositions in the relaxor region have shown that the transformation of the pseudocubic phase to the rhombohedral phase can be correlated with the temperature  $T_f$ , at which remanent polarization and coercive fields are first observed on cooling. The temperatures of the onset of this transformation are thus delineated by including a plot of known values of  $T_f$  in Fig. 5. However, the lack of pertinent  $T_f$  data means that it cannot be established at the present time whether this  $T_f$  plot will intersect the MPB, or the  $T_\alpha$  plot, at higher PT compositions.

The X-ray diffraction profiles in Figs. 2 & 3 clearly demonstrate that the structural phase transformations in the PMN-PT ceramic system do not go to completion at their respective initiation temperatures. Each solid line drawn in Fig. 5 thus represents a boundary between a high temperature phase and a two phase region, within which the phase transformation progresses (not necessarily linearly) with decreasing temperature. Hence, for completeness a further set of lines should be drawn on the diagram to represent the finish of the respective phase transformations, but no data are available to perform this operation at the present time. However, even if the finishing temperatures of the phase transformations were inserted in Fig. 5, it would still not conform to the Phase Rule. A similar situation was encountered several years ago with respect to the Fe-Ni alloy system, in which diffusion is very slow at temperatures below 500 °C, so that under normal heating and cooling conditions the  $\gamma$  to  $\alpha$  phase transformation occurs by a martensitic mechanism, as opposed to diffusion controlled nucleation and growth. While a proper phase diagram has been developed by annealing samples for very long periods [24], it is of limited practical use because the defined microstructures are not obtained by normal industrial heat treatments. The start and finish temperatures of the phase transformation during heating and cooling at normal rates have thus been used to develop a so-called "realization diagram" [24], by which microstructures can be predicted under normal conditions. A similar realization diagram for the PMN-PT system can be developed from accurate determinations of the transformation start and finish

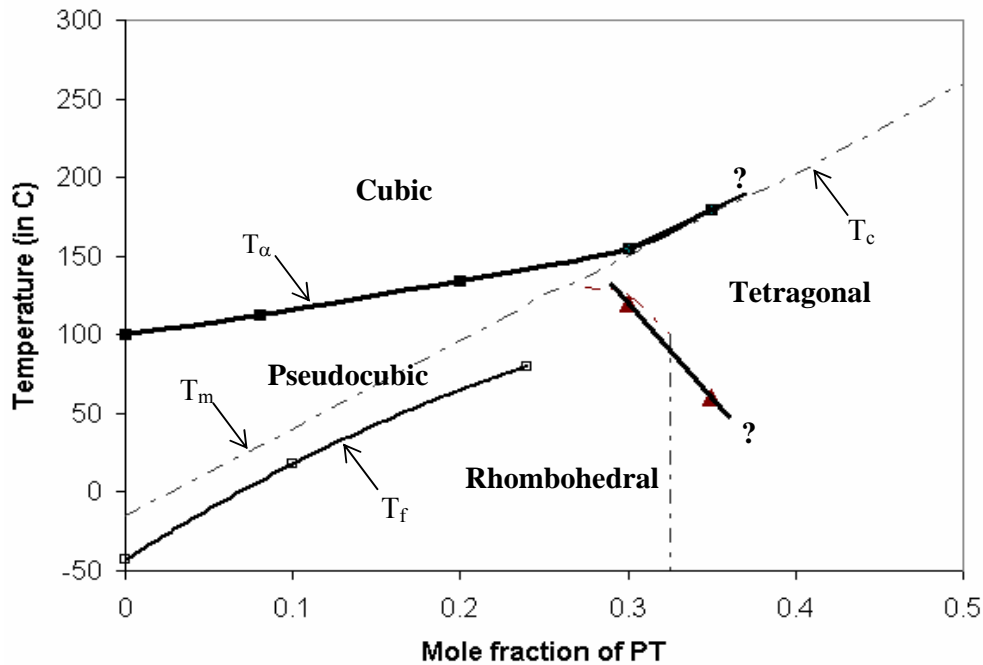


Figure 5. Structural phases and dielectric transitions in PMN-PT ceramic system.

temperatures of additional compositions across the relaxor, MPB and piezoelectric regions. Such a diagram would also include the temperature dependence of the dielectric transitions, and thus provide a useful resource for those involved in the development of sonar sensors and smart materials.

#### ACKNOWLEDGEMENTS

The authors acknowledge the support of the Natural Science and Engineering Research Council of Canada, the Office of Naval Research, USA, and the Department of National Defence, Canada.

#### REFERENCES

1. G.A. Smolensky, "Physical Phenomena in Ferroelectrics with Diffuse Phase Transition", *J. Phys. Soc. Japan*, **28**(Supp.), 26-36 (1970).
2. K. Orchino, S. Nomura, L.E. Cross, S.J. Jang and R.E. Newnham, "Electrostrictive effect in lead magnesium niobate single crystals", *J. Appl. Phys.*, **51**(2), 1142-1145 (1980).
3. L.E. Cross, L.E., "Relaxor Ferroelectrics: An Overview", *Ferroelectrics*, **151**, 305 (1994).
4. R.E. Newnham, V. Sundar, R. Yimnurun, J. Su and Q.M. Zhang, "Electrostriction in Dielectric Materials", *Ceramic Trans.*, **88**, 15-39 (1998).
5. S.W. Choi, T.R. Shrout, S.J. Jang and A.S. Bhalla, "Dielectric and Pyroelectric Properties in the  $\text{Pb}(\text{Mg}_{1/3}\text{Nb}_{2/3})\text{O}_3\text{-PbTiO}_3$  System", *Ferroelectrics*, **100**, 29-38 (1989).
6. J-C. Shaw, K-S. Liu and I-N. Lin, "Dielectric Behavior at Morphotropic Phase boundary for PMN-PZT Ceramics", *Scripta Metall. et Material.*, **29**, 981-986 (1993).
7. J.C. Ho, K.S. Liu and I.N. Lin, "Study of ferroelectricity in the PMN-PT system near the morphotropic phase boundary", *J. Mater. Sci.*, **28**, 4497-4502 (1993).
8. Feigelson, (2002),  
[www: hhttp://.www-mse.stanford.edu/people/faculty/feigelson/projects/PMNT/PMNhome]
9. F. Chu, I.M. Reaney and N. Setter, "Investigation of Relaxors that Transform Spontaneously into Ferroelectrics", *Ferroelectrics*, **151**, 343-348 (1994).

10. D. Viehland and J.F. Li, "Investigations of electrostrictive  $\text{Pb}(\text{Mg}_{1/3}\text{Nb}_{2/3})\text{O}_3\text{-PbTiO}_3$  ceramics under high-power drive conditions: Importance of compositional fluctuations on residual hysteresis", *J. Appl. Phys.*, **89**(3), 1826-1835 (2001).
11. X. Guishing, H. Luo, P. Wang, Q. Zhenyi and Y. Zhiwen, "Ferroelectric phase transition in relaxor ferroelectric single crystals 0.76PMN-0.24PT", *Chinese Science Bull.*, **45**(15) 1380-1385 (2000).
12. S.L. Swartz, T.R. Shrout, W.A. Schulze and L.E. Cross, *J. Amer. Ceram. Soc.*, **67**, 311, (1984).
13. S.M. Gupta and A.R. Kulkarni, "Synthesis of Perovskite Lead Magnesium Niobate using Partial Oxalate Method", *Mat. Res. Bull.*, **28**, 1295-1301 (1993).
14. M. Villegas, J.R. Jurado, C. Moure and P. Duran, "Processing and properties of  $\text{Pb}(\text{Mg}_{1/3}\text{Nb}_{2/3})\text{O}_3\text{-PbZrO}_3\text{-PbTiO}_3$  ceramic relaxors", *J. Mater. Sci.*, **29**, 1090-1096 (1994).
15. R. Zhang, S. Peng, D. Xiao, Y. Wang, B. Yang, J. Zhu, P. Yu and W. Zhang, "Preparation and Characterization of  $(1-x)\text{Pb}(\text{Mg}_{1/3}\text{Nb}_{2/3})\text{O}_3\text{-xPbTiO}_3$  Electrocalorific Ceramics", *Cryst. Res. Technol.*, **33**(5), 827-832 (1998).
16. D.S. Paik and S. Komarneni, "Composites of  $0.9\text{Pb}(\text{Mg}_{1/3}\text{Nb}_{2/3})\text{O}_3\text{-}0.1\text{PbTiO}_3$  prepared by a sol-gel method: effect of atmospheric powders", *J. Mater. Sci.*, **34**, 2313-2317 (1999).
17. D.F. Waechter, D. Liufu, M. Camirand, R. Blacow and S.E. Prasad, "Development of High-Strain Low Hysteresis Actuators Using Electrostrictive Lead Magnesium Niobate (PMN)", *Proc. 3<sup>rd</sup>. CanSmart Workshop on Smart Materials and Structures*, (Montreal, 2000) pp.31-36.
18. "NCEMT Contributes to LBVDS Passing Sea Test", *Metal Working Technology, Update*, (Concurrent Technologies Corporation, Johnstown, PA 15904-1935, Summer 2002).
19. H.W. King, S.H. Ferguson, D.F. Waechter and S.E. Prasad, "X-ray Diffraction Study of PMN-PT Ceramics in the Region of the Relaxor Transition", *Proc. 2<sup>nd</sup> Canada-US CanSmart Workshop on Smart Materials and Structures*, (Montreal, December 10-12, 2002). pp.11-20, ISBN 0-9685840-3-9.
20. H.W. King and E.A. Payzant, "Error Corrections for X-ray Powder Diffractometry", *Canad. Metall. Quart.*, **40**(3), 385-394 (2001).
21. S. Kojima and F. Jiang, "Broadband Brillouin Scattering of Relaxor Ferroelectric Crystals", (2002), [[www http://particle.physics.wm.edu/ferro2001\\_papers/06\\_Kojima.pdf](http://particle.physics.wm.edu/ferro2001_papers/06_Kojima.pdf)]
22. L.E. Cross, "Dielectric, Piezoelectric and Ferroelectric Compounds", *Ceramic Bull.*, **63**, 586-590 (1994).
23. "Powder Diffraction File PDF 2, Release 2002", International Center for Diffraction Data (ICDD), Newton Square, PA 19073-3273, USA. (2001).
24. M. Hansen and K. Anderko, *Constitution of Binary Alloys*, (McGraw-Hill Book Co., New York, 1958), pp. 677-684.